Turbulence Associated With Broadband Shock Noise in Hot Jets

James E. Bridges and Mark P. Wernet
Glenn Research Center, Cleveland, Ohio

NASA STI Program . . . in Profile

Since its founding, NASA has been dedicated to the advancement of aeronautics and space science. The NASA Scientific and Technical Information (STI) program plays a key part in helping NASA maintain this important role.

The NASA STI Program operates under the auspices of the Agency Chief Information Officer. It collects, organizes, provides for archiving, and disseminates NASA's STI. The NASA STI program provides access to the NASA Aeronautics and Space Database and its public interface, the NASA Technical Reports Server, thus providing one of the largest collections of aeronautical and space science STI in the world. Results are published in both non-NASA channels and by NASA in the NASA STI Report Series, which includes the following report types:

- TECHNICAL PUBLICATION. Reports of completed research or a major significant phase of research that present the results of NASA programs and include extensive data or theoretical analysis. Includes compilations of significant scientific and technical data and information deemed to be of continuing reference value. NASA counterpart of peer-reviewed formal professional papers but has less stringent limitations on manuscript length and extent of graphic presentations.

- TECHNICAL MEMORANDUM. Scientific and technical findings that are preliminary or of specialized interest, e.g., quick release reports, working papers, and bibliographies that contain minimal annotation. Does not contain extensive analysis.

- CONTRACTOR REPORT. Scientific and technical findings by NASA-sponsored contractors and grantees.

- CONFERENCE PUBLICATION. Collected papers from scientific and technical conferences, symposia, seminars, or other meetings sponsored or cosponsored by NASA.

- SPECIAL PUBLICATION. Scientific, technical, or historical information from NASA programs, projects, and missions, often concerned with subjects having substantial public interest.

- TECHNICAL TRANSLATION. English-language translations of foreign scientific and technical material pertinent to NASA's mission.

Specialized services also include creating custom thesauri, building customized databases, organizing and publishing research results.

For more information about the NASA STI program, see the following:

- Access the NASA STI program home page at *http://www.sti.nasa.gov*

- E-mail your question via the Internet to *help@ sti.nasa.gov*

- Fax your question to the NASA STI Help Desk at 301–621–0134

- Telephone the NASA STI Help Desk at 301–621–0390

- Write to:
  NASA Center for AeroSpace Information (CASI)
  7115 Standard Drive
  Hanover, MD 21076–1320

Turbulence Associated With Broadband Shock Noise in Hot Jets

James E. Bridges and Mark P. Wernet
Glenn Research Center, Cleveland, Ohio

National Aeronautics and
Space Administration

Glenn Research Center
Cleveland, Ohio 44135

September 2008

Acknowledgments

This work was supported by the Supersonics Project of the Fundamental Aeronautics Program.

Level of Review: This material has been technically reviewed by technical management.

Available from

Turbulence Associated With Broadband Shock Noise in Hot Jets

James E. Bridges and Mark P. Wernet
National Aeronautics and Space Administration
Glenn Research Center
Cleveland, Ohio 44135

Time-Resolved Particle Image Velocimetry (TRPIV) has been applied to a series of jet flows to measure turbulence statistics associated with broadband shock-associated noise (BBSN). Data were acquired in jets of Mach numbers 1.05, 1.185, and 1.4 at different temperatures. Both convergent and ideally expanded nozzles were tested, along with a convergent nozzle modified to minimize screech. Key findings include the effect of heat on shock structure and jet decay, the increase in turbulent velocity when screech is present, and the relative lack of spectral detail associated with the enhanced turbulence.

Introduction

Of all the jet noise source mechanisms, broadband shock-associated noise (BBSN) is relatively well understood. The basic concept of correlated undulations of shocks by convecting turbulence, codified first by Harper-Bourne and Fisher[1] and later by Tam[2,3], has proven robust and useful for predicting the noise from round jets. The elaborate extension to rectangular jets[4] was made more difficult by the need for more complicated analysis of instabilities in the rectangular jet, but was satisfactory as well. However, the general problem of predicting BBSN from a generic three-dimensional nozzle remains.

Efforts to develop a statistical prediction code for BBSN based upon Reynolds-Averaged Navier-Stokes (RANS) CFD will require validation of assumptions and models used in the development. Such prediction code development also requires that the turbulent flow solution to be used as input be checked for accuracy. For computational simplicity an axisymmetric cold jet would be preferred as a base case for development. However, cold axisymmetric jets typically have some degree of screech, which has been observed to amplify the entire spectra, as demonstrated by Tanna[5]. RANS CFD solutions cannot predict the time-dependent resonance of screech. Therefore, it is important to develop test cases for BBSN that do not include screech and to understand the role of screech in modifying the turbulence and its influence on BBSN.

Screech is a well-understood resonance phenomena involving growth of jet column instability waves, acoustic emission from interactions of the instability waves with the shocks in the jet column, and receptivity of the acoustic emission at the nozzle lip initiating the instability waves (see reference [3] for a good quick overview). Previous efforts to remove screech have attacked either the axisymmetry of the jet (modifying the jet flow, typically with tabs, to change the instability characteristics) [5], or the receptivity (arranging reflectors to exactly cancel the acoustic tone at the nozzle lip) [6,7]. The former is unsuitable if one wants to retain axisymmetry for theoretical and computational convenience. The latter is cumbersome as reflectors must be modified for each flow condition. One other important jet parameter also removes screech: high jet temperatures [8]. As the jet is heated, the jet velocity increases. The preferred frequency of the instability wave decreases while that of the resonant acoustic wave given by the shock cell geometry remains fixed. At sufficient temperature, the jet ceases to screech while retaining its broadband shock noise. Unfortunately, the jet mixing noise, which increases with jet velocity, begins to overshadow the BBSN, making separation of the BBSN and mixing noise more difficult.

It is thought that the best way to separate mixing noise and BBSN is to measure the noise of a comparable shock-free jet flow, assume that the noise is totally due to turbulent mixing, and furthermore

assume that this mixing noise is the same spectrally in the shocked jet. These assumptions would be greatly bolstered if it could be shown that the turbulent flow field, arguably the defining aspect of the mixing noise source, was the same for both fully expanded and shocked jets. Further complicating matters, we have found that even nozzles designed to have ideally expanded divergent sections invariably have a small residual pressure imbalance which gives rise to a disproportionately large amount of broadband shock noise. Measures of even the small shocks should be made to account for the small amount of BBSN present in these nearly shock-free flows.

All these issues require detailed measurement of the turbulence in supersonic jets, with and without screech, at various temperatures and with varying degrees of shock strength.

Of course, measurement of turbulence in high speed jets, especially hot jets which are of most technological interest, is very difficult with conventional anemometry such as hotwires, or even laser Doppler anemometry. Modern particle image velocimetry (PIV) now allows such measurements to be made with relative ease. Standard low frequency PIV can provide such measures as mean and rms velocities in the jet plumes, and even purely spatial correlations that can support models of turbulence coherence used in the BBSN modeling[9]. With the recent development[10] of time-resolved particle image velocimetry (TRPIV) much more information can be obtained, including turbulence spectra around the shocks, full space-time correlation of the turbulence over the shocks, and even the oscillation of the shocks with the passing of turbulent structures. Such an experimental study has been undertaken at NASA Glenn Research Center and the initial results will be reported in this paper.

To further demonstrate the motivation and design of the experiments, consider the far-field noise of a convergent nozzle operated at an ideally expanded Mach number M of 1.18, with varying temperature. Shown in Figure 1 are the power spectral density as observed at 100 jet diameters broadside (90°) and downstream (140°) from the jet. The different temperatures give rise to different velocities, which when normalized by ambient speed of sound yield acoustic Mach numbers from 1.18 to 1.8. The peak jet mixing noise is noted at $St_D = 0.2 - 0.3$, while the broadband shock noise is observed in the 90° data around $St_D = 1$. Due to the multiple screech modes present at this M, many tones are evident for the lower temperature jets, disappearing at the highest temperature due to mismatches between the most amplified instability wave and the feedback frequencies [11]. To a remarkable degree, the jet mixing noise is increasing with temperature /velocity while the shock-associated noise is relatively unchanged. All flows should have had the same shock structure, having the same Mach number, so this is mostly expected.
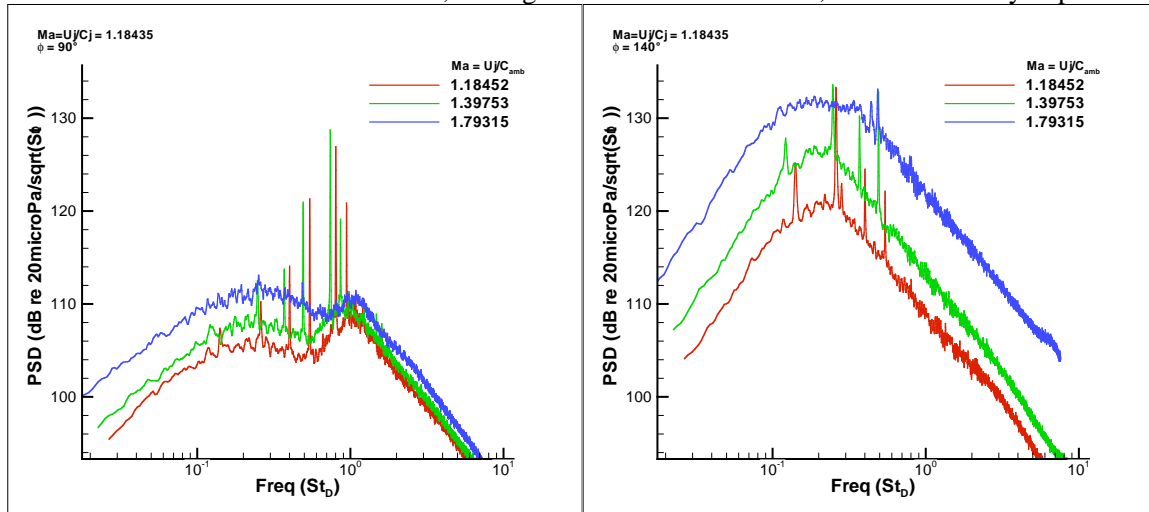

Figure 1 Far-field noise spectra at 90° (left) and 140° (right) to the jet downstream axis. M = Uj/cj = 1.18; Ma = 1.18 (isothermal), 1.4 (static temperature ratio 1.4), and 1.8 (static temperature ratio = 2.37).

An appealing simplification has been to assume that the jet turbulence is independent of the shocks, and that the broadband shock noise is produced by turbulence which is unaffected by the shocks. There is, however, the question of whether the shocks do modify the turbulent jet structure. Answering this

question, along with other subtle aspects of shock-turbulence interaction, has led to a major investigation of the turbulence of hot supersonic jets, both with and with shocks, and with shocks but without screech.

When investigating the impact of various flow parameters, normalizations help in making comparisons. In this work, velocities are normalized by the ideally expanded jet velocity U_{id}, dimensions are normalized primarily by jet exit diameter D_j, and frequencies are presented in $St_D = f*D_j/U_{id}$. When comparing jets with different spread rates and potential core lengths, dimensions are often normalized by the potential core length. The prediction for potential core length X_w, given by Witze [12] is a good starting point, but is actually only applicable for fully expanded jets, as will be demonstrated below. For the purposes of collapsing data from the convergent nozzles, the potential core length was determined from data and designated X_c. A subsequent normalization of the jet radius was found to hold for the fully expanded jets and will be employed below. Y_c was defined as the half-velocity radius at the end of the potential core. In much the same spirit as Witze's original work, Y_c was correlated to density ratio, surprisingly with the same exponent as that for X_w: $Y_c/D_j = 0.574 (\rho_j/\rho_\infty)^{-0.22}$. Tables of these values will be given below.

Facilities, Instrumentation, and Test Matrix

Small Hot Jet Acoustic Rig (SHJAR)

The Small Hot Jet Acoustic Rig (SHJAR), located within the AeroAcoustic Propulsion Laboratory (AAPL) at NASA's John H. Glenn Research Center, is a single-stream hot jet rig. The AAPL is a 65 foot radius geodesic dome with its interior covered by sound absorbent wedges that provide the anechoic environment required to study propulsion noise from the several rigs that are located within. The jet rigs are positioned such that they exhaust out the open doorway, allowing the flows to be seeded and removing issues related to background noise from flow collectors. Bridges & Brown[13] contains more information on the facility and jet rig. In typical testing, the SHJAR can cover the range of Mach numbers up to Mach 2, and static temperature ratios up to 2.8 using a hydrogen combustor and central air compressor facilities. For most testing SHJAR uses a 50.8mm (2 inch) diameter nozzle, but can operate larger nozzles with some limitation on cold setpoints at high Mach number. Total flow conditions for the rig are measured in the large plenum 0.6m upstream of the nozzle. Figure 2 gives a sketch of the rig.
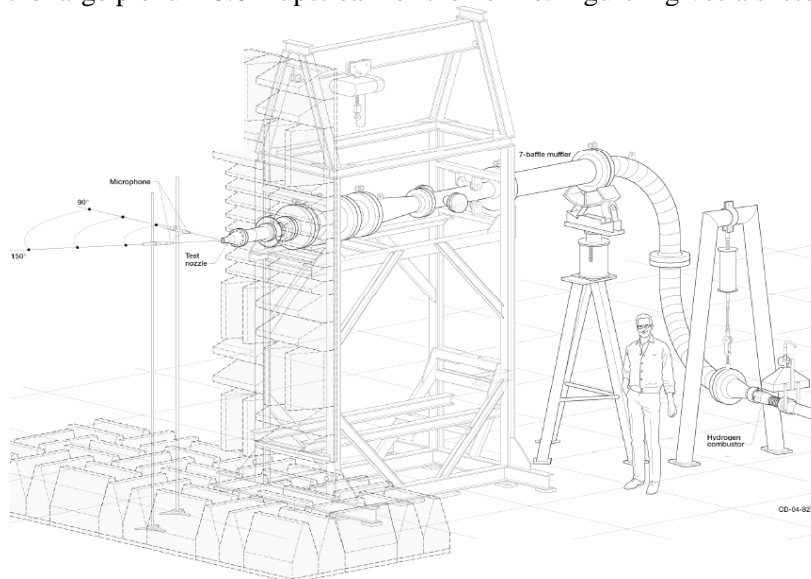

Figure 2 Small Hot Jet Acoustic Rig in typical acoustic configuration.

TRPIV

In essence, Time-Resolved Particle Image Velocimetry (TRPIV) is very similar to standard PIV with two exceptions. First, the camera is configured to store only the portion of the image required, minimizing

the amount of information stored to only those regions of interest. The camera has on-board storage to record the images locally, saving the time-consuming (roughly 600 times slower) part of downloading data to computer storage until after the acquisition is complete. The camera acquires images at a rate twice that of the final data recording rate, with each pair being used to construct one velocity vector field, until the cameras' 4 gigabyte storage capacities are filled. The camera is synchronized with a pair of high repetition pulsed lasers that each fire at the final data recording rate, and with a time interval between lasers that is inversely proportional to the maximum velocity and correlation region of the image. Image processing is done using mostly the same correlation-based methods as in standard PIV, but having sequential velocity fields allows some additional checking of the vector field validity. In the final analysis, good seeding is the key to having fully populated vector fields essential for unbiased statistics. Full details of the TRPIV system are found in [10].

In this application of TRPIV, data was acquired primarily at 10kHz sample rate, although several cases were acquired at 25kHz over smaller fields of view to confirm the high frequency roll off of point spectra). Two identical cameras were used to double the field of view available. When temporal correlations are performed on the data, the correlations will remain significant over several diameters as coherent structures advected downstream. For this reason, the field of view was optimized for a long narrow strip of flow approximately $0.5D_j$ high by $6D_j$ long. One set of data was acquired centered on the nozzle centerline and another set acquired centered on the nozzle lip line. The two sets did not overlap radially. More importantly, each set was acquired at different offsets downstream, allowing data to be acquired from roughly $1 < x/D_j < 20$. Figure 3 illustrates the regions of the flow acquired in physical space. Because of the high aspect ratio of the measurement region, many figures are presented in the Results section with the radial coordinate greatly expanded.
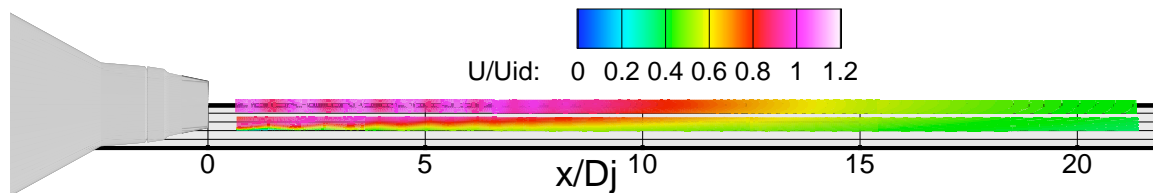

Figure 3 Locations of TRPIV acquisitions. Six overlapping fields of 6 diameters apiece produce the total measurement region.
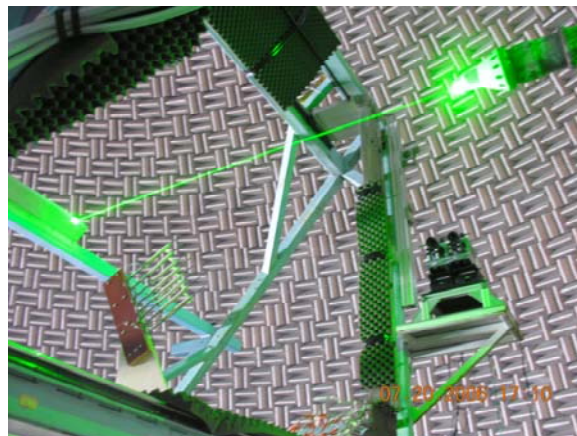

Figure 4 Picture of TRPIV setup in SHJAR. Beam introduced from covered optics directly downstream of nozzle, directed at nozzle lip, upper right. Dual cameras, lower right, record particle images at right angles to beam.

Figure 4 is a photo of the final configuration for measuring along the nozzle lip line, with the beam-forming optics contained within a sheet metal box, and the laser sheet emerging directly downstream of the nozzle lip. The dual cameras can be seen in the picture, viewing the beam from right angles and recording the first 6 jet diameters together. The beam-forming optics were kept clean by pressurizing the

sheet metal box so that air came out the beam opening at a velocity higher than the jet at that downstream location. Before this air was added the optics became too dirty to use within a few seconds of seeding the flow. After the addition of the purge air the optics stayed clean for several acquisitions, or a few minutes.

Hardware and Test Matrix

For this study three different nozzles were used, a convergent nozzle and two convergent-divergent (fully expanded) nozzles, all with exit diameters of 50.8mm (Figure 6). The fully expanded nozzles were designed using the method of characteristics and confirmed with RANS CFD to provide nearly ideal expansion of the flow before the nozzle exit. Two design Mach numbers were tested, M_d=1.185 and 1.40. By heating the jet, a matrix of conditions were established, alternately varying the Mach number ($M=U_j/C_j$) and the acoustic Mach number ($Ma=U_j/C_\infty$), as given in Table 1, and schematically in Figure 5. At each flow condition plume measurements were made with both fully expanded and simple convergent nozzles.
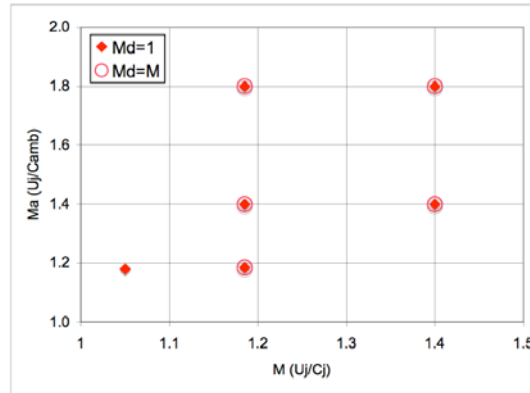

Figure 5 Test condition matrix

Table 1 Setpoint definitions for test matrix.

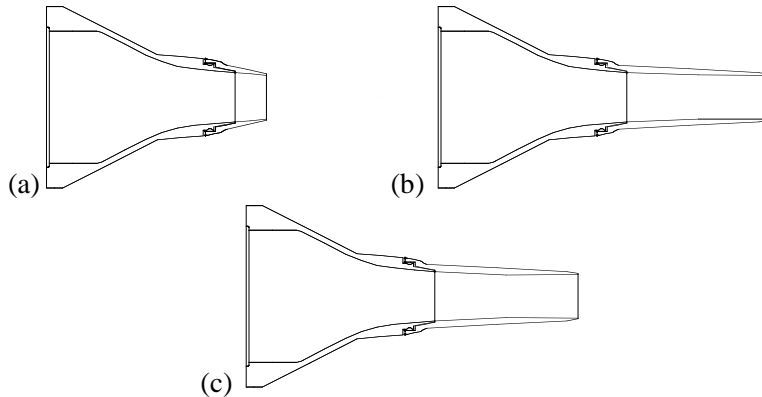| Setpoint	M	Ma	T_s/T_∞	U_j (m/s)
7030	1.05	1.180	1.266	405.39
8020	1.185	1.185	1.000	407.10
8030	1.185	1.400	1.401	480.97
8060	1.185	1.800	2.368	618.39
9020	1.4	1.400	1.000	480.97
9050	1.4	1.800	1.665	618.39

Figure 6 Nozzles (a) SMC000 ($M_d = 1.0$), (b) SMC014 ($M_d = 1.185$), (c) SMC015 ($M_d = 1.4$) used in study.

Figure 7 Convergent nozzle SMC000 (left) and modified convergent nozzle SMC021 (right).

Although the convergent-divergent nozzles were designed to give ideally expanded flow using the method of characteristics, the impact of boundary layers and nozzle lip thickness make it very difficult, perhaps impossible, to achieve a flow where the Mach number is exactly unity across the nozzle exit and no pressure imbalances exist throughout the jet. In practice, the minimum shock Mach number was established for each nozzle by finding the flow condition with the minimum shock noise and screech. This was different from the design condition by about less than 0.5%, and the exact Mach number was held as the temperature (and hence acoustic Mach number) were varied.

In an attempt to obtain a round jet without screech, several iterations on nozzle lip geometry were attempted. Starting with an axisymmetric nozzle, such as that on the left in Figure 7, modifications were made on the nozzle, first on outer surface, then radically tripping the boundary layer, without significant impact on the screech. Finally, cutting the small notches as seen on the right in Figure 7 produced a jet with barely perceptible screech. The degree of deviation from axisymmetry was minimal, at least compared to the tabbed jets often studied. Measurements were made in a plane between notches.

Results

Fully Expanded Nozzle Flow

Fully expanded jet flows are well-behaved and the mean and mean square velocities can be shown to collapse well with appropriate normalization. By first considering the flow from fully expanded nozzles, the interesting aspects of shocked jets that give rise to shock-associated noise are more evident. As an overview, consider the plots of mean axial velocity U/U_{id} in Figure 8 and mean square axial velocity $\overline{uu}/U_{id}^2$ in Figure 9.

The plots are very similar in topology and amplitude, varying only in spatial dimensions. There are only slight shocks from the not-quite-perfect expansions of the jet at the nozzle exit. Normalizing the axial and radial coordinates to account for the impact of jet density on jet mixing, the data collapse very nicely. To do this normalization, the data are plotted in x/X_c and y/Y_c where

$$\frac{x}{X_c} = \frac{\left(x/D_j\right)}{\left(X_c/D_j\right)}$$

$$\frac{y}{Y_c} = \frac{\left(y/D_j\right)}{\left(1 + 2\left(x/X_c\right)\left(\left(Y_c/D_j\right) - 0.5\right)\right)}.$$

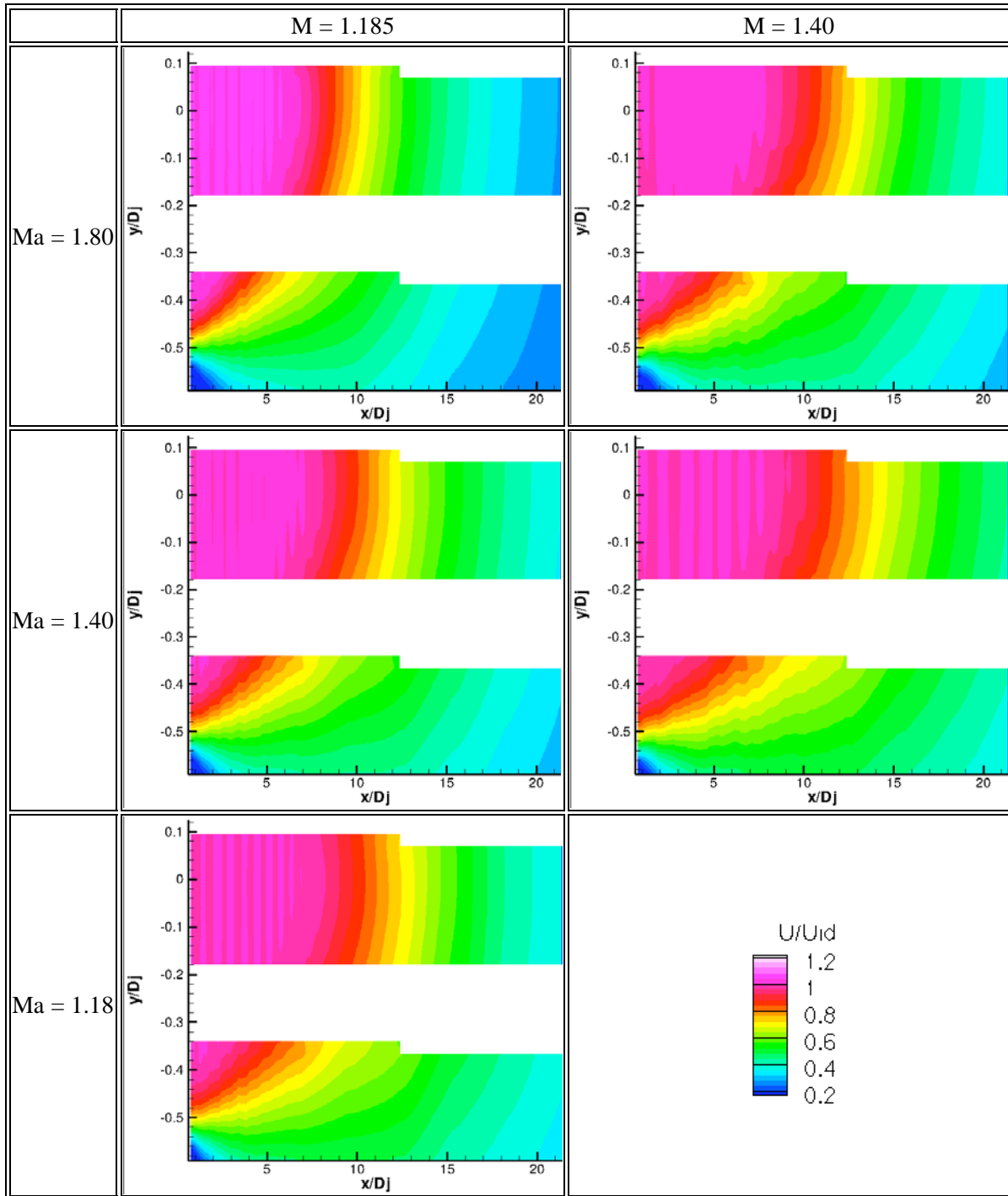|	M = 1.185	M = 1.40
Ma = 1.80		
Ma = 1.40		
Ma = 1.18		

Figure 8 Plots of mean axial velocity U/U_{id} *at different* $M = U_j/c_j$ *and different* $Ma = U_j/c_\infty$ *for fully expanded nozzle flows.*
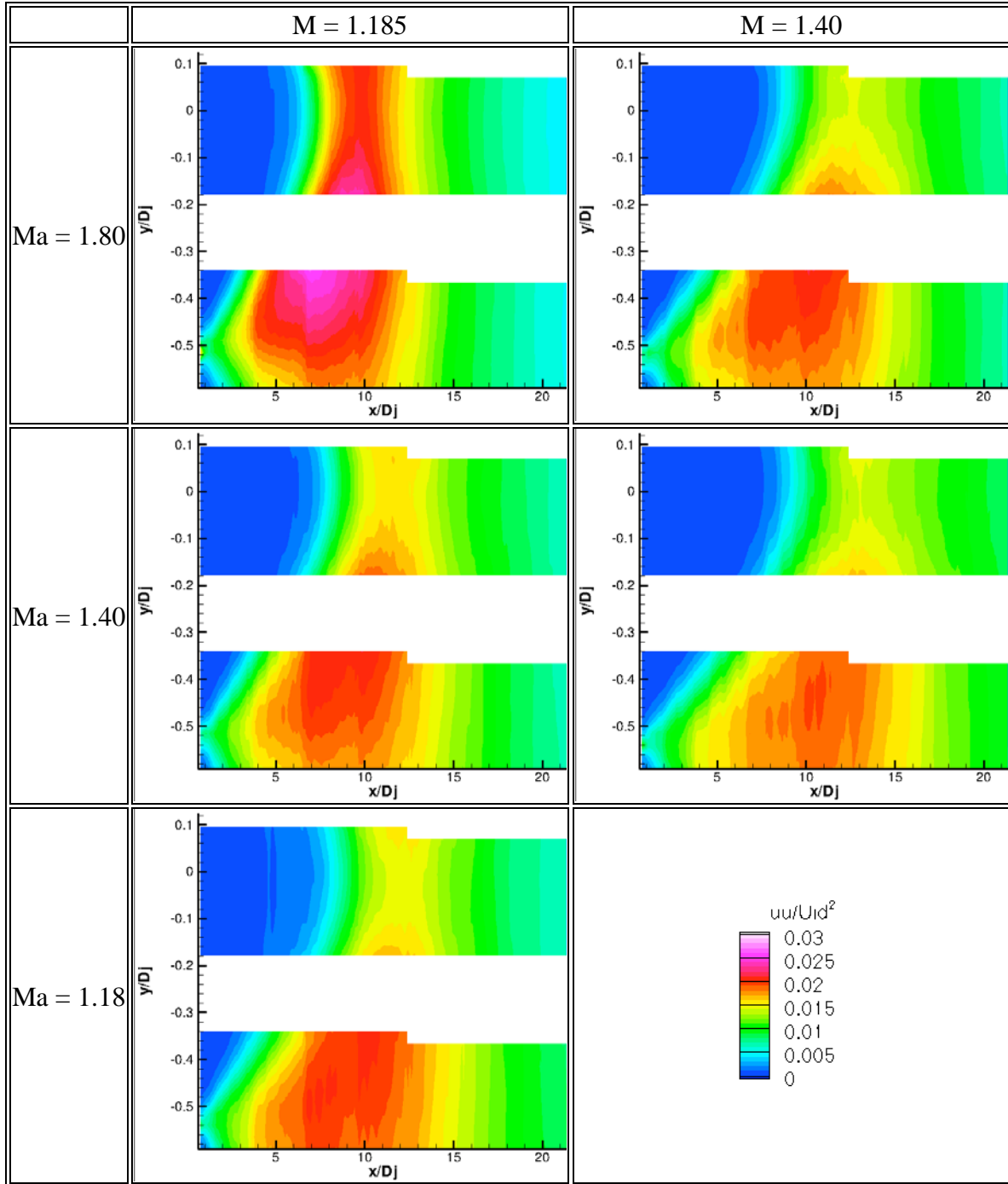
Figure 9 Plots of mean square axial velocity $\overline{uu}/U_{id}^2$ at different M and Ma for fully expanded nozzle flows.

As mentioned above, the X_c is the potential core length, which is nicely given by Witze's correlation [12] in the case of fully expanded jets, while Y_c is the half-velocity radius at the end of the potential core and was found to correlate with jet density ratio, $Y_c/D_j = 0.574\,(\rho_j/\rho_\infty)^{-0.22}$ for the five cases measured here. Figure 10 demonstrates this by first showing contour plots of axial mean velocity U/U_{id} near the jet lipline for all the flow cases in physical coordinates $(x/D_j, y/D_j)$ (left hand plot). Each flow is represented by a set of contour lines, the color of each flow given by the legend. The same data are replotted in x/X_c, y/Y_c coordinates in the right hand plot. The amount of warping created by the normalizations is evident in

the mapping of the rectangular measurement domain on the left plot to the various curved boxes on the right. The warping of different flows can be determined by their colors. The disorganized mess of contour lines in the physical space plots resolve into tidy bundles in the warped plot, demonstrating the collapse of the data using the X_c, Y_c normalization. Note in particular how, by design, the contour line for $U/U_{id} = 0.5$ follows $y/Y_c = 0.5$ over the range $0 < x/X_c < 1$.
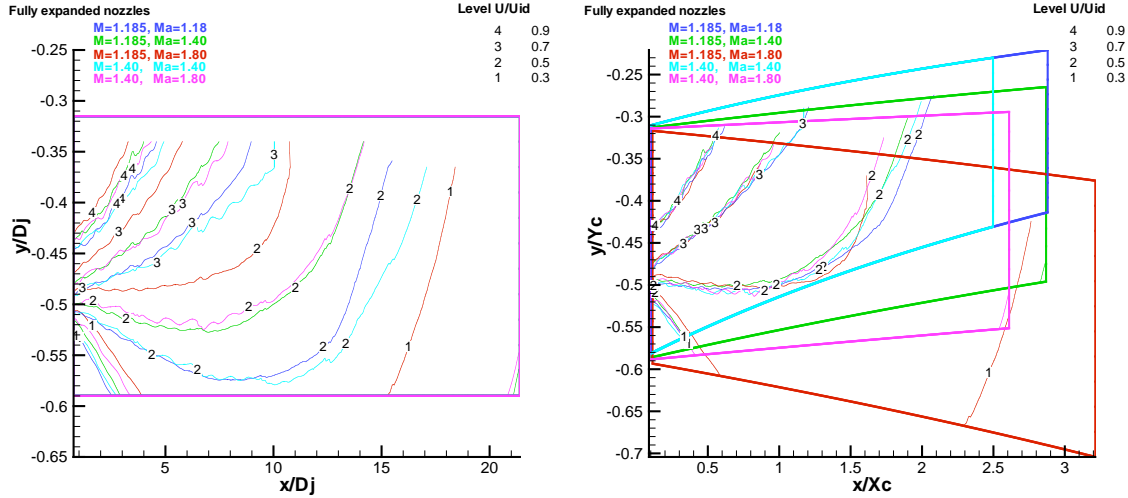

Figure 10 Contour plots of mean axial velocity U/U_{id} *for different flow conditions, plotted in spatial coordinates (x/D$_j$, y/D$_j$) left, and in normalized coordinates (x/X$_c$, y/Y$_c$) right.*

The measurements of the mean square of axial velocity $\overline{uu}/U_{id}^2$ also collapse to roughly a single shape when plotted on x/X_c, y/Y_c coordinates, as shown in Figure 11. The peak turbulence level has a broad peak around $x/X_c = 1.3$, or just downstream of the end of the potential core. Radially, the peak is near $y/Y_c = 0.4$, or to the high speed side of the shear layer. It seems noteworthy that these are features of subsonic jets as well.
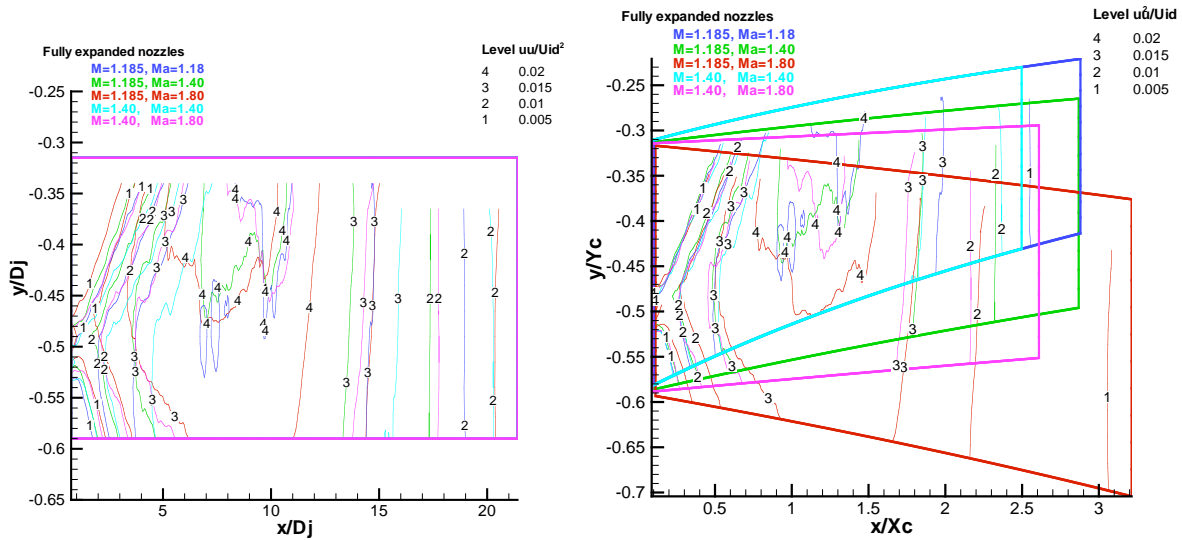

Figure 11 Contour plots of mean square axial velocity $\overline{uu}/U_{id}^2$ *for different flow conditions, plotted in spatial coordinates (x/D$_j$, y/D$_j$) left, and in normalized coordinates (x/X$_c$, y/Y$_c$) right.*

By studying which flow conditions are warped in which direction it is clear that heating the jet causes the jet to mix faster, shortening the potential core and causing the half-velocity point to move inward. Increasing the Mach number retards the mixing, lengthening the potential core. Given that heating

decreases the jet density for a given fully-expanded velocity, while increased Mach number increases the jet density, it is to be expected that a collapse based upon density ratio would hold.

To better illustrate the collapse of data for the fully expanded jets, consider cuts through the normalized space at the jet centerline ($y/Y_c = 0$; Figure 12) and the normalized lip line ($y/Y_c = 0.5$; Figure 13). Clearly, the axial normalization caused the jet centerline data to collapse in this coordinate along the centerline. The only quantity that does not fully collapse is the turbulent velocity; the mean square of the velocity is significantly higher in the case of the hottest jet. The turbulent velocity does collapse for data on the normalized lip line $y/Y_c = 0.5$, however. It appears that as the half-velocity line and the peak of the turbulence is moved inward with increased heating of the jet, the turbulence intensity also increases on the centerline.
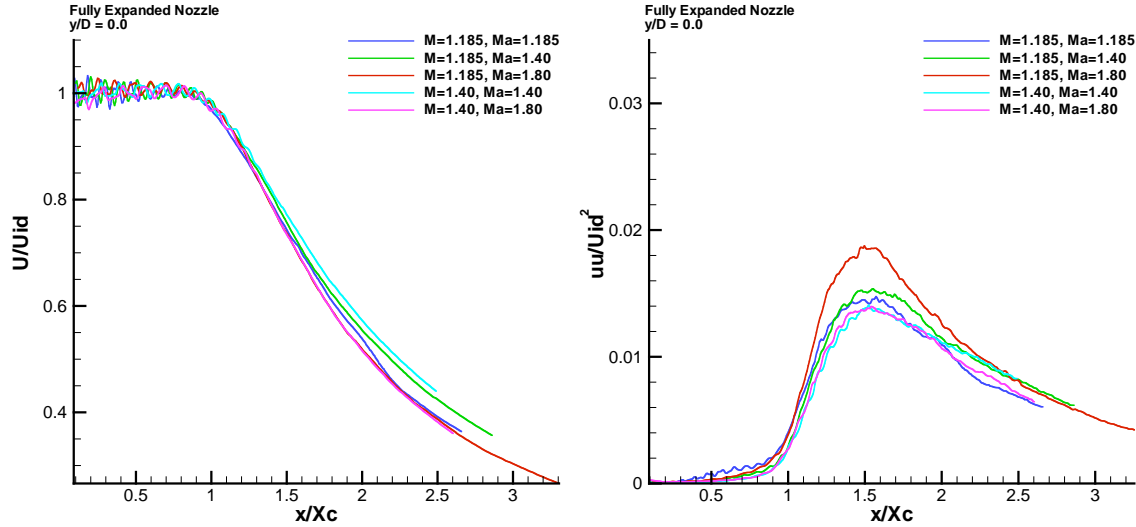

Figure 12 Mean axial velocity (left) and mean square axial velocity (right) on centerline for all fully expanded nozzles, plotted in normalized coordinates.
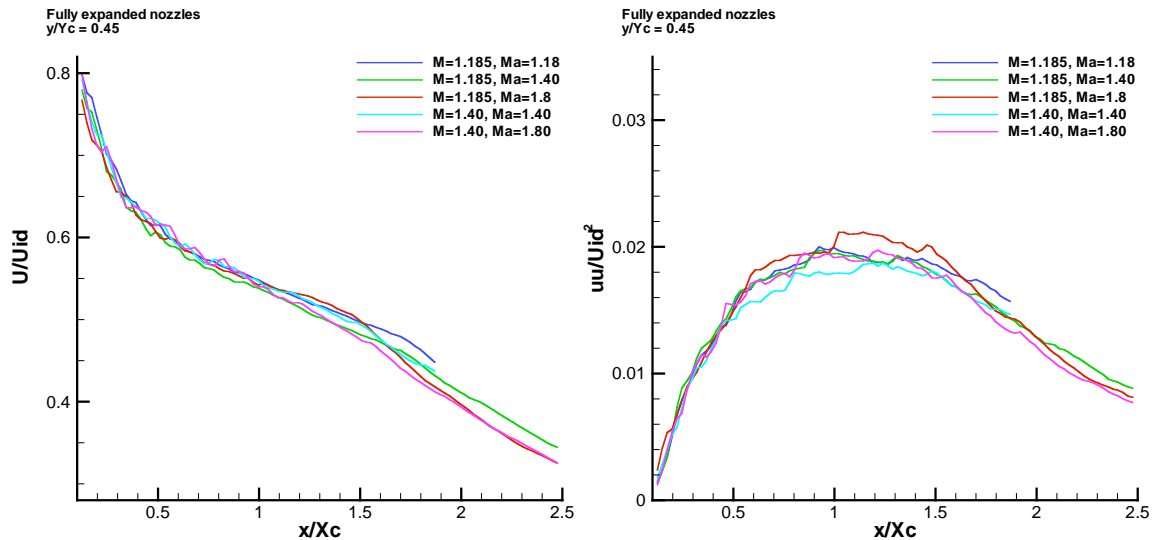

Figure 13 Mean axial velocity (left) and mean square axial velocity (right) on normalized lipline ($y/Y_c = 0.5$) for all fully expanded nozzles, plotted in normalized coordinates.

Spectrally, the jet turbulence is rather undistinguished and can be summarized by considering the spectra along the physical jet centerline and lip line. Each plot of Figure 14 shows power spectral density

of axial velocity (Guu, in dB re U_j) plotted against frequency (Strouhal number in log scale) and axial location (in x/D_j) for the indicated radial locations, centerline and lipline. Although the spectra were specifically measured in an isothermal M = 1.4 jet, the findings are typical of all the fully expanded jets measured. On the centerline, the frequency content of the turbulence is very broadband, with a slightly elevated amplitude at frequencies at or above $St_D = 0.5$ throughout the potential core. Of course, the amplitude of these fluctuations are very small, being in the potential core. The steady rise in the turbulence at the end of the potential core is very broadband over the frequency domain shown, until just before the peak turbulence level is reached. At this point, there is a distinct high frequency roll off for x/$X_c > 1$ that decreases roughly as 1/x. The spectra does not have a peak near $St_D = 0.3$, instead being flat or monotonic at every axial station beyond the potential core. On the lip line the results are very similar—the turbulence spectra at any given axial station is flat to a frequency beyond that measured up until the end of the potential core when an high frequency develops and changes with axial distance as 1/x.

Having completed the tour of the fully expanded jet, the convergent jet will be considered next. Two related phenomena cause these flows to be much more complicated: shocks and screech.
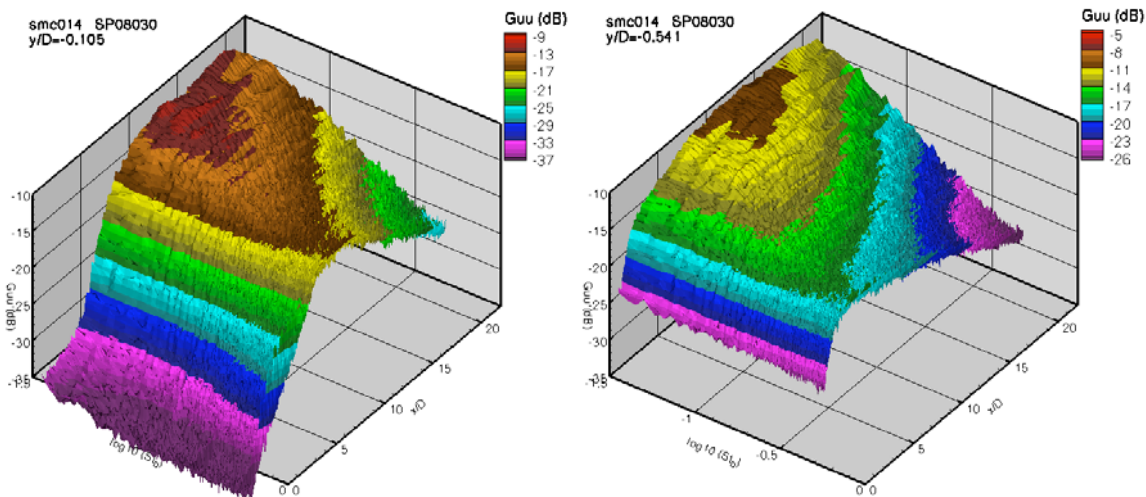

Figure 14 Power spectral density of axial velocity on centerline (left) and lip line (right) of fully expanded jet operating at M = 1.4, Ma = 1.4. Power spectral density is plotted against frequency (log St_D) and axial distance downstream.

Underexpanded Jets

Analysis of the convergent nozzle flows begins with an overview of the mean and mean square velocity fields, presented in Figure 15 and Figure 16, respectively. The shocks are readily apparent in the mean flow fields, growing stronger with increased M, but becoming very weak at the highest temperature case, Ma = 1.8. at M = 1.18. By inspection the potential core lengths do not follow the expected pattern based on jet momentum. So we see that the potential core length increased while heating the M=1.4 jet from Ma = 1.4 to Ma = 1.8.

There is large discrepancy in the turbulence levels between different flow conditions, and all are higher than in the fully expanded jets with the same flow conditions. For example, the turbulence level found in the M = 1.18, Ma = 1.18 is 50% higher than in the same flow with fully expanded flow nozzle. The turbulence levels are strongly modulated by the shocks.
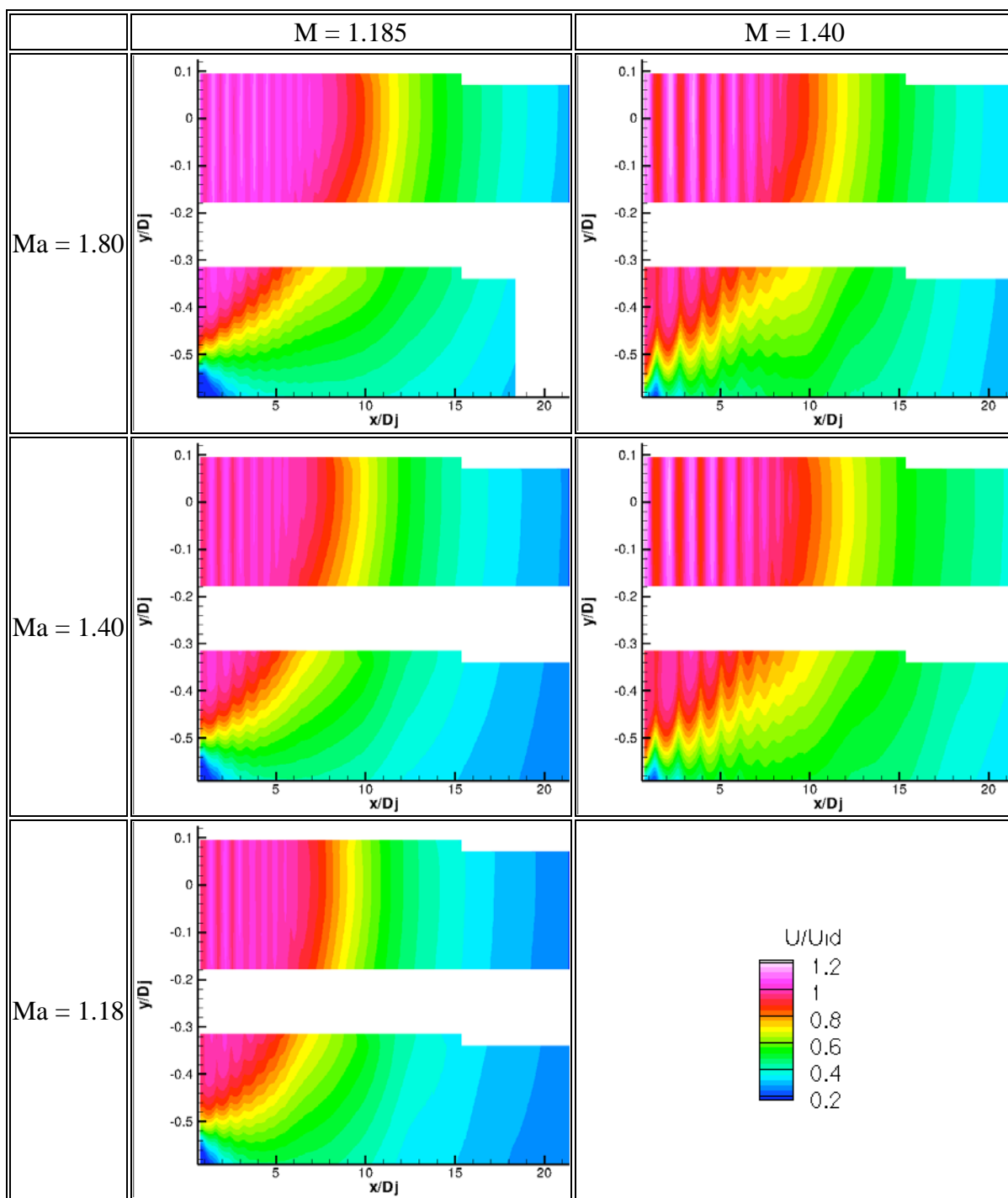
Figure 15 Plots of mean axial velocity U/U$_{id}$ at different M = U$_j$/c$_j$ and different Ma = U$_j$/c$_\infty$ for convergent nozzle flows.
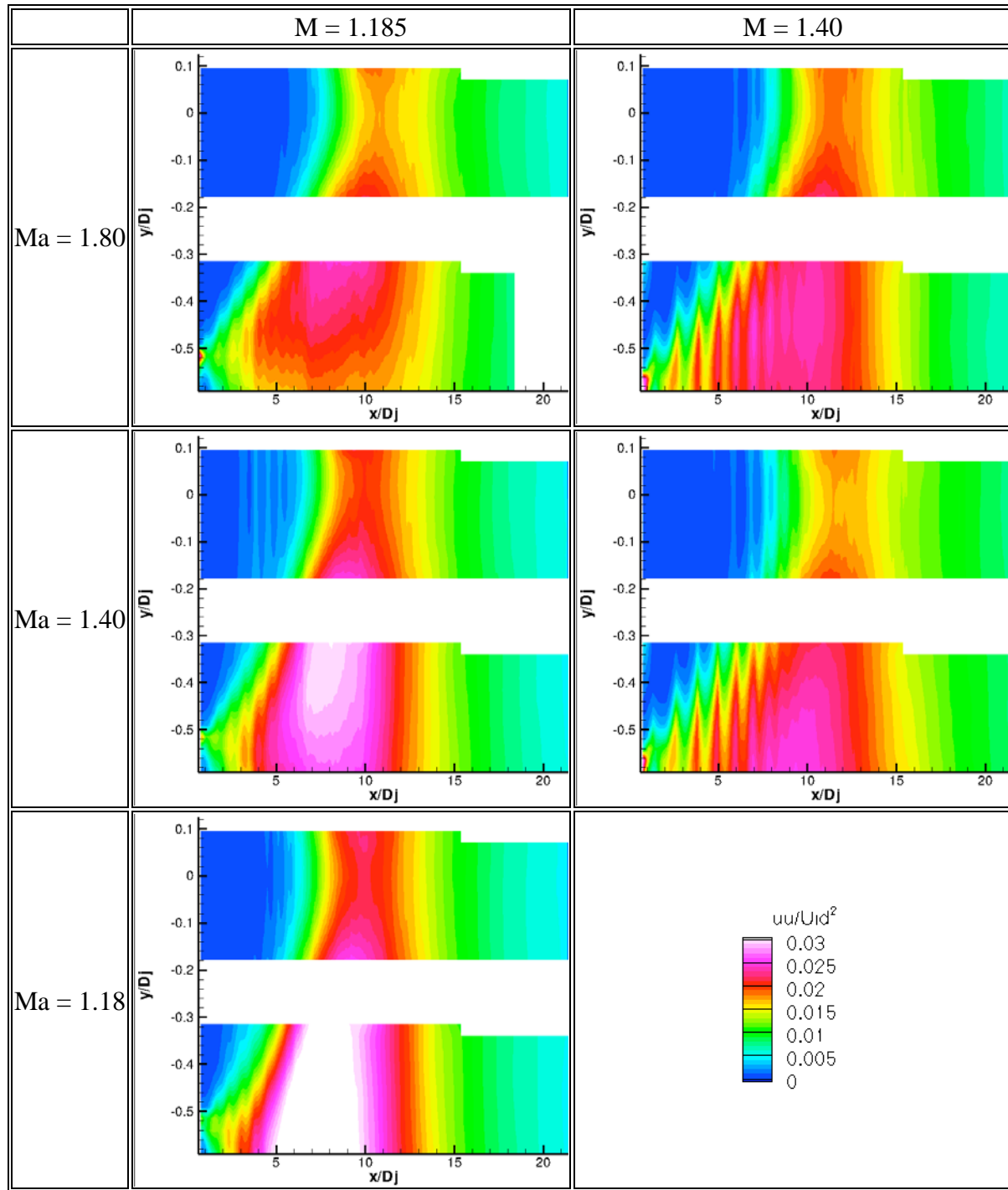
Figure 16 Plots of mean square axial velocity uu/U_{id}^2 at different M = U_j/c_j and different Ma = U_j/c_∞ for convergent nozzle flows.

A rough normalization of the axial coordinate was determined by aligning the turbulence peaks on the jet centerline so that they matched those of the fully expanded nozzle flows, as shown in Figure 17. This did not optimally align the mean centerline decay, as evident by the lack of collapse in the U/U_{id} in Figure 17. The values of X_c used for the convergent nozzle flows are given in Table 2 and are noticeably different from the Witze values. As seen in Figure 17, aligning the axial location of the potential core does not cause the collapse of the turbulence fields in amplitude. This is especially true for the peak

turbulence, located on the lip line, Figure 18. From the figures it appears that, for a given M, increased temperature decreased the peak turbulence levels.

The significance of this observation is apparent when one remembers that screech strength decreases with heating as the frequency of the most amplified instability wave and of the feedback begin to differ with increased heat. This is one indication of how screech changes the turbulent jet structure, causing such fundamental measures as potential core length and peak turbulence intensity to reverse their usual trends with Mach number and temperature.

One additional flow case, not acquired with a fully expanded nozzle, is a warm, M = 1.05 jet (setpoint 7030). This flow has very small shocks, with velocity undulations of 0.022U peak to peak in the potential core. The jet noise had no noticeable screech, and serves as a 'typical' subsonic jet flow for this comparison, comparing screeching jets with screech-free jets. Setpoint 7030 consistently had the lowest turbulence levels of all the flow conditions.

Table 2 Potential core lengths, in jet diameters, as used in report.

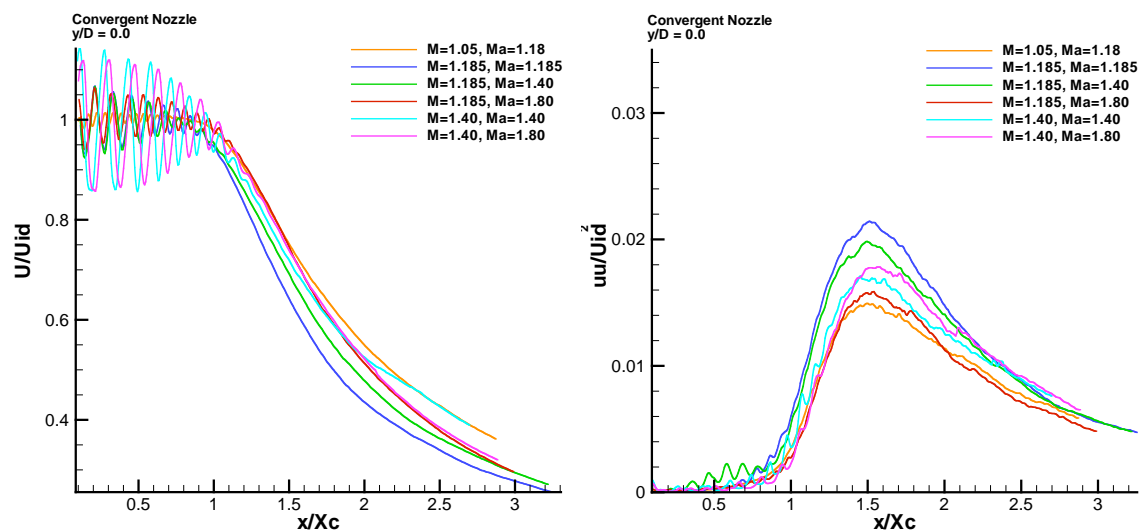| Setpoint	M	Ma	X_w/D_j Witze	X_c/D_j expt		
			Predicted	Convergent	Fully Expanded	Modified Convergent
7030	1.05	1.18	7.12	7.4		
8020	1.18	1.18	8.07	6.6	8	
8030	1.18	1.40	7.35	6.6	7.5	
8060	1.18	1.80	6.35	7.1	6.4	
9020	1.40	1.40	8.94	7.9	8.6	9
9050	1.40	1.80	7.75	7.5	8.2	

Figure 17 Mean axial velocity (left) and mean square axial velocity (right) on centerline for convergent nozzles, plotted in normalized coordinates.
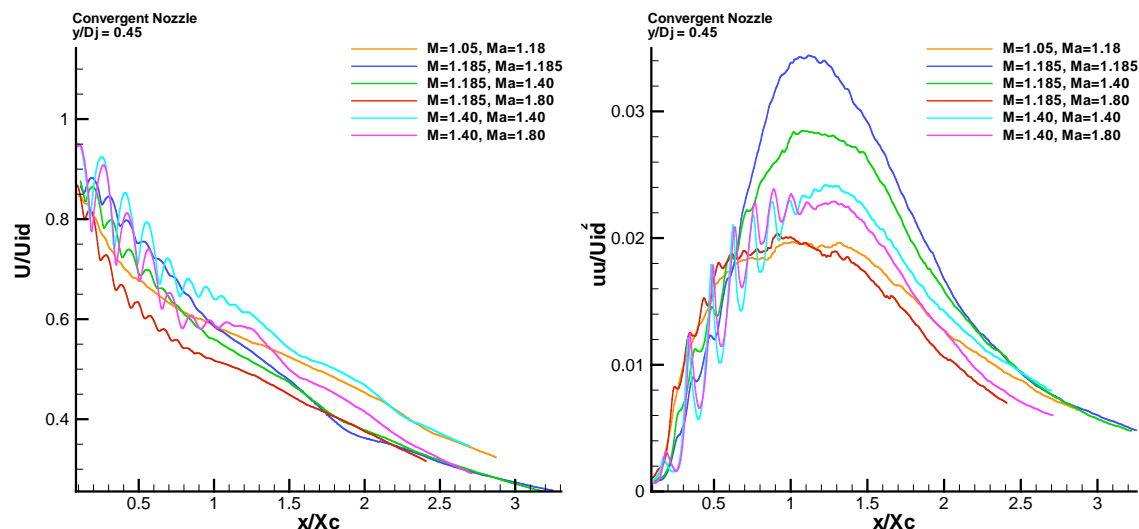
Figure 18 Mean axial velocity (left) and mean square axial velocity (right) on normalized lipline for convergent nozzles, plotted in normalized coordinates.

Velocity Spectra

The spectra of the convergent nozzle flows show several interesting features. One example is given in Figure 19 for M=1.4, Ma=1.4 jet flow for locations along the centerline and lip line. The first impression at this scale is that the spectra are very similar to those of the fully expanded jets. Riding atop this structure, however, is a tone at a very narrow band corresponding to the screech frequency. This tone is modulated by the shock structure and is quite strong in the potential core of the jet. The other very interesting feature is the modulation of the broadband turbulence by the shocks in the potential core region, as see in Figure 20. From this perspective one can discern the modulated broadband turbulence, apart from the modulated screech tone energy. This is especially apparent in the plot of spectra along the jet centerline, but is expected to be more important along the lip line where the turbulence is higher in amplitude and where theory says the turbulence is the source of broadband shock noise. A closer look at the relationship between shock and turbulence will be taken presently, but first consideration will be given to a shocked jet without screech.
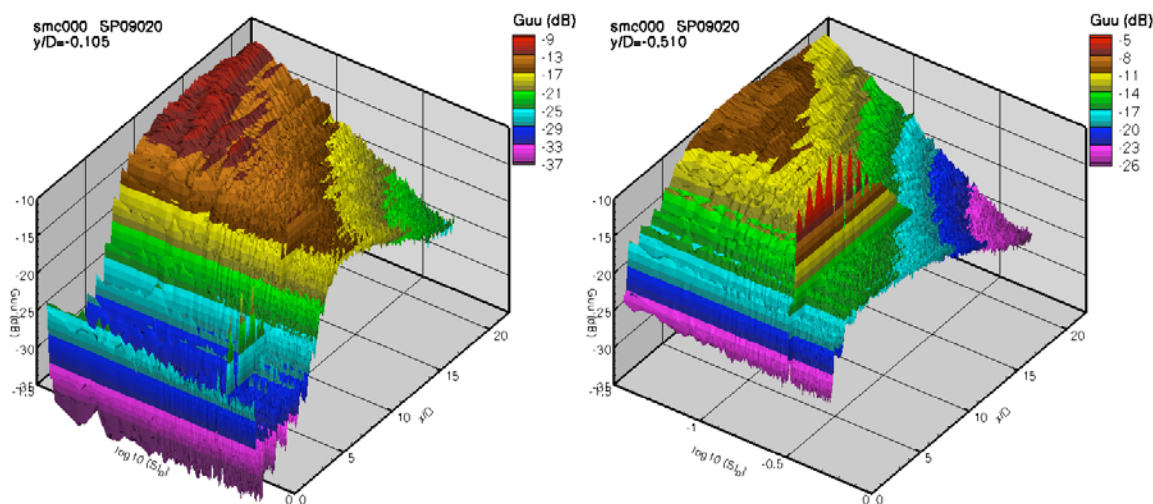

Figure 19 Power spectral density of axial velocity on centerline (left) and lip line (right) of convergent nozzle jet operating at M = 1.4, Ma = 1.4.
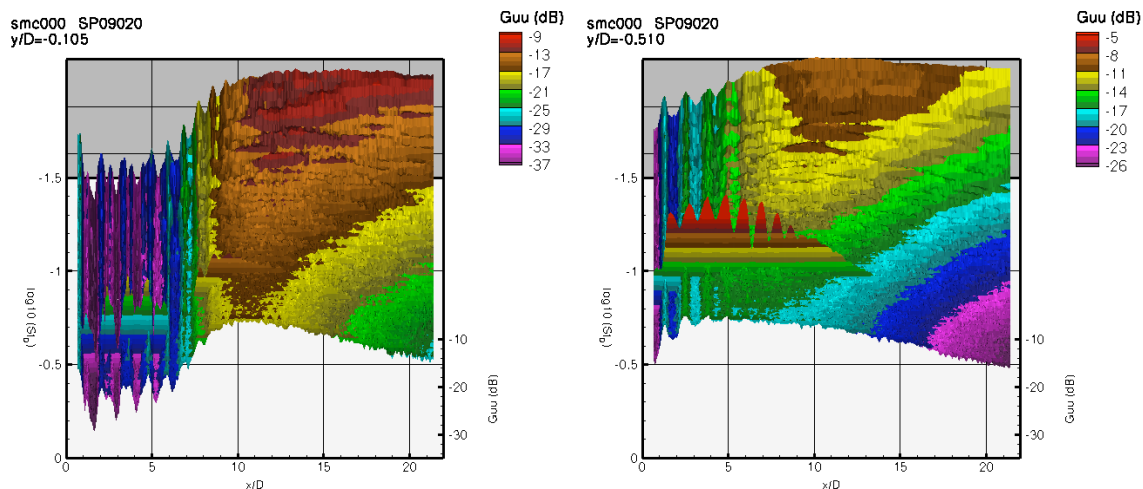
Figure 20 Power spectral density of axial velocity on centerline (left) and lip line (right) of convergent nozzle jet operating at M = 1.4, Ma = 1.4. Data is same as Figure 19, but viewed down the frequency axis.

To separate the effects of shock and screech, a modified convergent nozzle was studied for one flow condition, the M = 1.4, Ma = 1.4 jet (setpoint 9020). The modifications, shown in the Hardware section of this paper, caused the initial portion of the jet to have broken symmetry, delaying the initiation of the axisymmetric instability wave until after it had lost the connection in phase with the lip, and hence suppressing the feedback mechanism that gives rise to screech.

In Figure 21 the impact of the modifications on key statistics of the jet are noted. In the figure are plots comparing the centerline and lipline decay of the mean and mean square velocity for convergent, fully expanded, and modified convergent nozzles. In the plots one finds that the two convergent nozzles have very similar shock patterns, compared with the minimal shocks of the fully expanded nozzle. However, the modified nozzle has a potential core length and jet decay almost identical to the fully expanded nozzle. Moreover, the modified nozzle has similar turbulence levels in the potential core and at the peak. The flow quantities might be even more similar on the lip line if not for the fact that the shear layer of the convergent nozzle is actually farther outside the lip line because the jet quick expands to match pressures just downstream of the nozzle exit.

Hence the modified nozzle has shocks but otherwise has similar characteristics of a fully expanded jet. What is the key difference between the plain and modified convergent nozzle? In a word, screech.
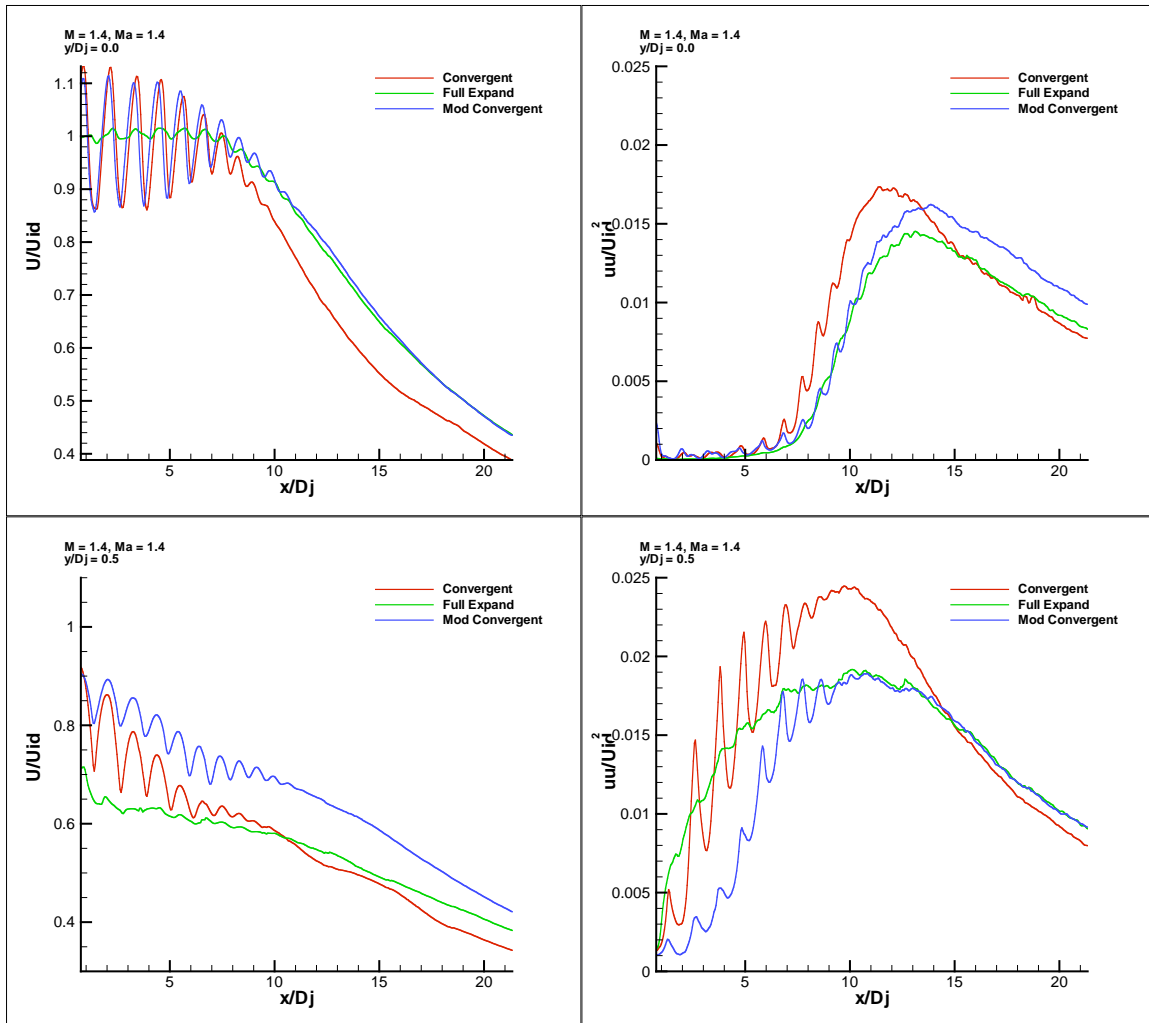
Figure 21 Mean axial velocity (left) and mean square axial velocity (right) along centerline (top) and along lip line (bottom) for convergent, fully expanded, and modified convergent nozzles at M = 1.4, Ma = 1.4.

From the far-field acoustic spectra of the convergent, modified convergent, and fully expanded nozzles, shown in Figure 22, one can discern that the modified convergent nozzle has the same broadband shock noise as the original convergent nozzle, but has much less screech and mixing noise. Simultaneously, it has low frequency mixing noise very close to that of the fully expanded, shock-free nozzle. That part of the jet flow that contributes to the broadband shock noise is the same for both convergent nozzles. The portion of the jet plume responsible for low frequency jet mixing noise is the same in the modified convergent nozzle and in the fully expanded nozzle flow. What has changed in the turbulence with the modifications to the convergent nozzle that retains the broadband shock noise but minimizes screech and retains the same mixing noise?
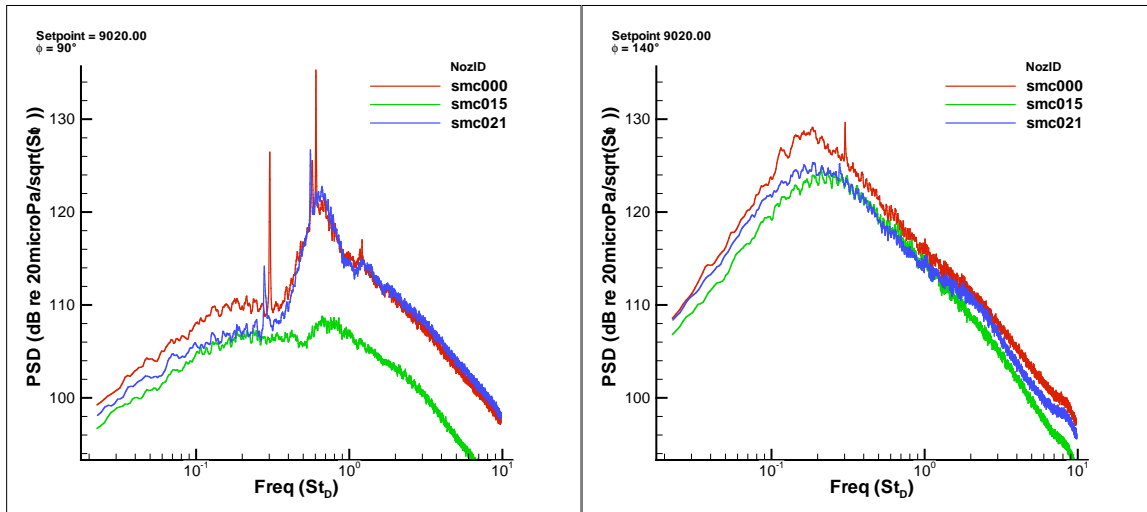
Figure 22 Far-field noise spectra at 90° (left) and 140° (right) to the jet downstream axis. M = 1.4; Ma = 1.4 for convergent, fully expanded, and modified convergent nozzles.
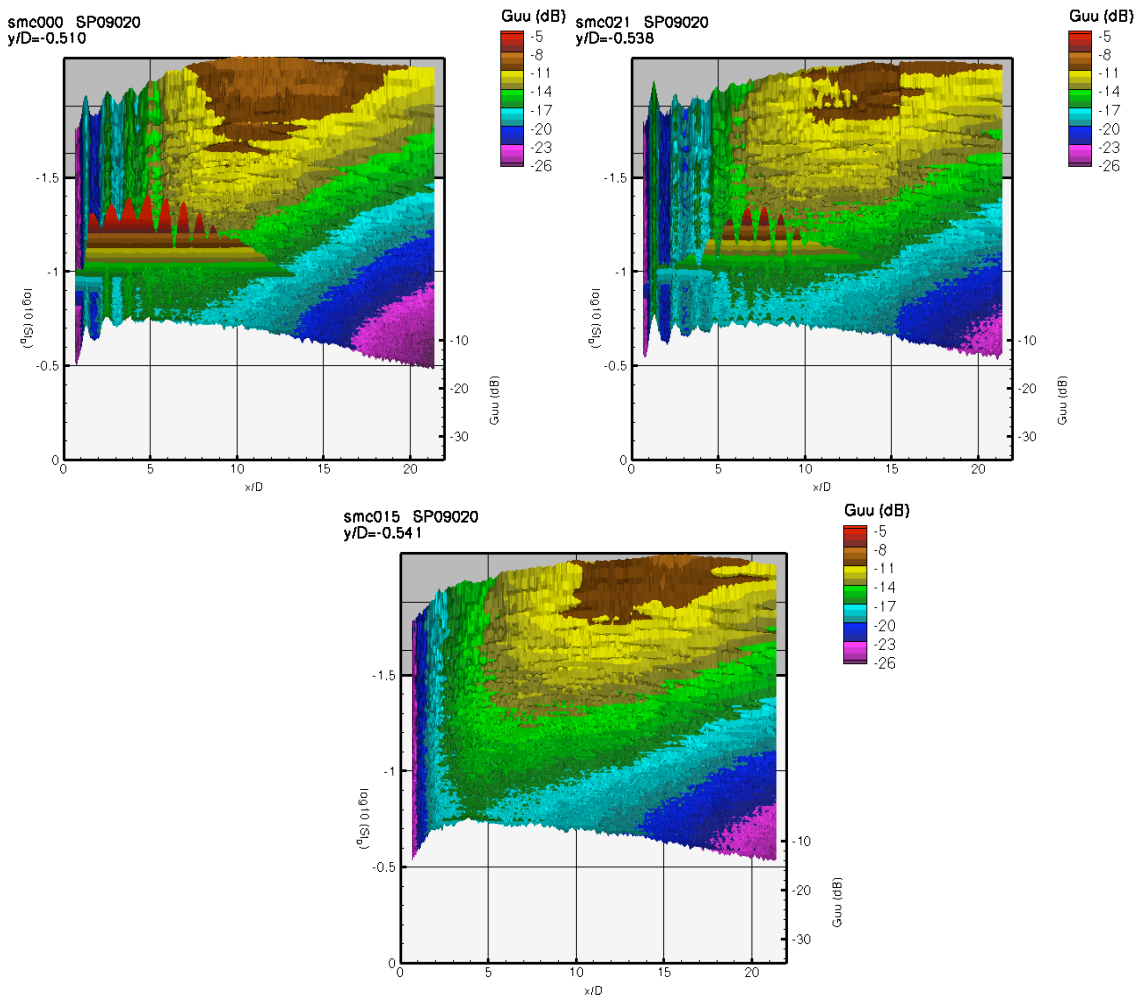

Figure 23 Power spectral density of axial velocity on lip line of convergent (left), modified convergent (right), and fully expanded (bottom) nozzles operating at M = 1.4, Ma = 1.4.

Figure 23 compares velocity spectral evolution along the lip line for the convergent, modified convergent, and fully expanded nozzles at M=1.4, Ma=1.4. The greatly diminished screech tone, which starts much farther downstream in the modified nozzle flow, is the most striking difference between the convergent nozzles. Next, one notices that the modulated turbulence along the potential core is very similar, although slightly reduced by the modification as well. And finally, the entire spectral level is slightly reduced overall, matching with the total mean square data shown in Figure 21. The reduced tone is consistent with the near lack of screech. Overall reduction in turbulence, especially at lower frequencies is consistent with the lower jet mixing noise. Interestingly, the broadband turbulence associated with the shocks is also reduced by the nozzle modifications, but the broadband noise that supposedly results from this turbulence is not. More could be made of this except that the velocity spectra only extends up to $St_D = 0.54$, barely reaching the low frequency end of the broadband shock noise.

Comparing the velocity spectra of the convergent nozzles with that of the fully expanded nozzle, the spectral shapes at any given axial station are very similar. The differences are due to overall turbulent energy just upstream of the potential core, as captured by the mean square profiles in Figure 21. Near the peak turbulence region just downstream of the potential core, the peak levels are within 1dB of each other and the spectra have the same roll off in both the modified convergent and fully expanded nozzle flows. Without the strong screech, the downstream development of the jet turbulence is unaffected.

To better compare the tones and broadband in the vicinity of the shocks, several frequency components are pulled from the spectra and plotted against the axial coordinate for the first 6 jet diameters. Figure 24 presents the spatial evolution of the axial and radial velocity components of screech tones on the lip line of the convergent and modified convergent nozzles. Each plot shows the mean axial velocity to locate the shocks, two lines for the axial and radial components of the tone, and two fuzzy sets of lines which are the axial and radial components of the broadband part of the spectra, uniformly sampled from $0.03<St_D<0.52$.

In the case of the convergent nozzle with screech, the axial and radial components of the tone are strong all along the potential core, and are modulated by the shocks. Downstream of $x/D_j = 3$ the radial and axial components of the tone are well synchronized to the shock structure: the radial component of the tone has a sharp drop near the shock (velocity minimum), the axial component of the tone is maximum just upstream of each shock. These relationships do not hold upstream of $x/D_j = 3$, where the tonal components are not as well synchronized with the shocks. For example, at $x/D_j = 2.6$ the radial component peaks at the shock while at $x/D_j = 3.8$ it has a deep null at the shock location. In the case of the modified convergent nozzle, the tone develops slowly from the levels of the broadband, presumably because little acoustic energy was being fed back to the lip. The axial and radial components of the tone have the same spatial relationship with the shocks as in the plain convergent nozzle where they are sufficiently strong to make out, e.g. $x/D_j > 3$.
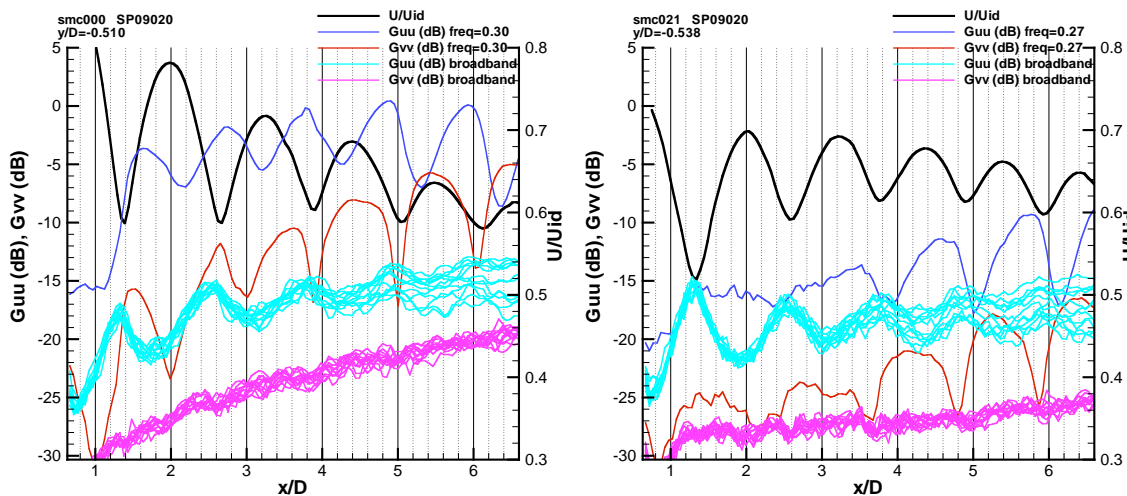

Figure 24 Spatial evolution of axial and radial velocity components of screech tones and of broadband levels along the jet lip line for M=1.4, Ma=1.4 flow from a convergent (left) and modified convergent (right) nozzle. Mean axial velocity is also plotted to give reference to the shock locations.

By contrast, the broadband axial component of turbulence is well-correlated with the shocks on the lip line over the entire potential core region peaking near the shocks for both nozzles. The broadband radial component of turbulence has very little modulation by the shocks, but is much greater in the plain convergent nozzle flow than in the modified nozzle flow. The difference in amplitudes of the broadband components between the two nozzles is partly because the spectra are taken along the geometric lipline while the maximum mean shear differs between the two nozzles.

Another spectral comparison of two improperly expanded jet flows, one with and without screech is shown in Figure 25. Here both flows issue from the plain convergent nozzle at the same Mach number (M=1.185), but the difference is in jet temperature—the hottest jet does not screech because of mismatch between instability wave frequency and feedback frequency. The sound spectra for these two flows were presented in Figure 1. These flows have a lower Mach number than the ones just presented in Figure 24, hence their shocks are not as strong. In the case of the lower temperature jet with screech, the screech tones are modulated by the shocks, but the broadband turbulence is only slightly modulated. The broadband turbulence is very comparable between the two flows, both in the axial and radial components. It does not appear that the presence of screech has a dramatic effect on the broadband turbulence, at least up to $St_D = 0.52$.
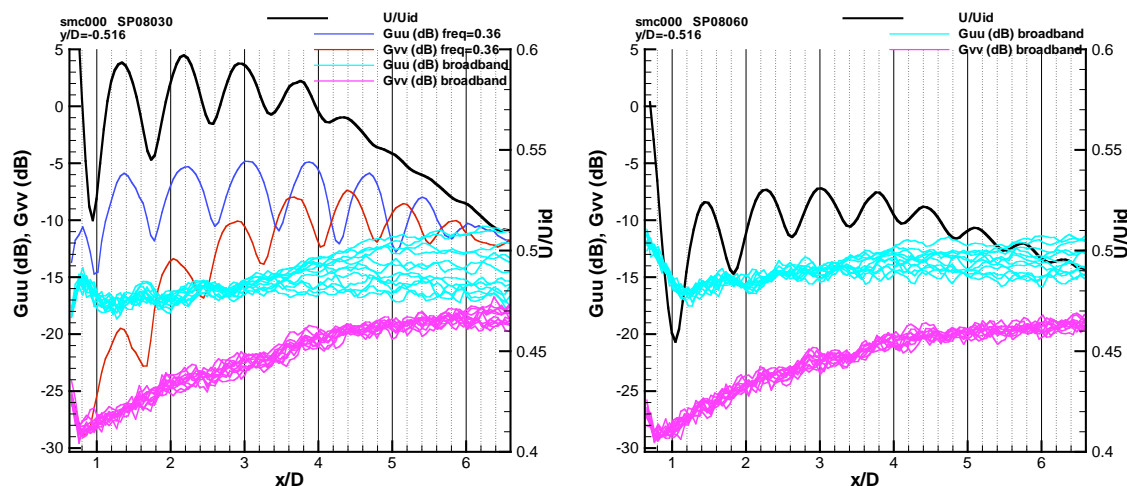

Figure 25 Spatial evolution of axial and radial velocity components of screech tones and of broadband levels along the jet lip line for M=1.185, Ma=1.4 (left) and Ma=1.8 (right) flows from a convergent nozzle. Mean axial velocity is also plotted to give reference to the shock locations.

The importance of these observations is in the modeling of the turbulence near shocks for broadband shock noise prediction. Clearly, the broadband turbulence is modified by the presence of shocks when they are of sufficient amplitude, independent of whether screech was a dominant feature or not. Spectrally, the screech tone appears to ride on the broadband spectrum without adding any spectral features. Aside from the obvious tone, the impact of screech is primarily imposed on the spreading of the jet and overall amplification of turbulence. This was surprising as nonlinear interactions in the turbulence usually result in spectral broadening, generation of harmonics and subharmonics, and other spectral features. More investigation will be required to understand whether the tone observed in the velocity spectra is vortical (turbulent) or irrotational (acoustic), and how the presence of the screech results in overall, broadband, amplification.

Conclusions

A new method of velocimetry, Time-Resolved Particle Image Velocimetry, has been deployed to obtain turbulence statistics of hot supersonic jets, including spectra. Analysis of new time-dependent turbulent velocity field data has shown that the impact of heat on the turbulence of fully expanded jets is mostly accountable by considering the change in momentum caused by the reduction in density of the hot jet. Normalization by axial and radial scales which correlate to density variations cause very good

collapse of the mean and mean square velocities for fully expanded hot jets. When the jets are not fully expanded and shocks are present, the presence and strength of screech overrules the density factor in determining the mixing of the jet. In shocked jets, the influence of heating on shock structure appears negligible at least for temperature ratios under 3; the ideally expanded Mach number determines the shock spacing independent of jet temperature. Given the strong influence of screech on the development of turbulence and the difficulty removing screech while retaining an axisymmetric jet, acquiring baseline data for a round shocked jet to be simulated by a time-independent numerical code is very difficult, if not impossible. The best practical flow that satisfies these requirements is a shocked, round jet heated sufficiently, say above static temperature ratio 2.5, where resonance is precluded. Data for such a case has been acquired in this study.

References

[1] Harper-Bourne, M. and Fisher, M.J,. "The noise from shock waves in supersonic jets," *AGARD-CP-131* 11:1-13 (1974).

[2] Tam, C.K.W., "Stochastic model theory of broadband shock associated noise from supersonic jets," *J. Sound Vib* **116**, 265-302 (1987).

[3] Tam, C.K.W., "Supersonic jet noise," *Ann Rev Fluid Mech* **27**, 17-43 (1995).

[4] Tam, C.K.W., "The shock cell structure and screech tone frequency of rectangular and non-axisymmetric supersonic jets," *J. Sound Vib* **121**, 135-147 (1988).

[5] Tanna, H.K., "An experimental study of jet noise, Part II: shock associated noise," *J. Sound Vib* **50**, 429-444 (1977).

[6] Nagel, R.T., Denham, J.W. and Papathanasiou, A.G. "Supersonic jet screech tone cancellation," *AIAAJ* **21**, 1541-1545 (1983).

[7] Khan, T.I., Seto, K., Xu, Z. and Ohta, H. "An approach to noise reduction of a supersonic jet with a spherical reflector," *Acoust. Sci. & Tech*. **25**, 136-143 (2004)

[8] Tam, C.K.W., Ahuja, K.K., and Jones III, R.R, "Screech tones from free and ducted supersonic jets," *AIAAJ* 32, 917-922 (1994).

[9] Bridges, J., "Effect of heat on space-time correlations in jets," *AIAA Paper 2006-2534* (2006).

[10] Wernet, M.P., "Temporally resolved PIV for space–time correlations in both cold and hot jet flows," *Meas. Sci. Technol.* **18**, 1387–1403 (2007).

[11] Tam, C.K.W., Chen, P. and Seiner, J.M., "Relationship between instability waves and noise of high-speed jets," *AIAAJ* **30**, 1747-1752 (1992).

[12] Witze, P.O., "Centerline velocity decay of compressible free jets," *AIAAJ* Vol **12**(4), 417-418 (1974).

[13] Brown, C.A., & Bridges, J., "Acoustic efficiency of azimuthal modes in jet noise using chevron nozzles," *AIAA-2006-2645* (2006).

REPORT DOCUMENTATION PAGE

Form Approved
OMB No. 0704-0188

The public reporting burden for this collection of information is estimated to average 1 hour per response, including the time for reviewing instructions, searching existing data sources, gathering and maintaining the data needed, and completing and reviewing the collection of information. Send comments regarding this burden estimate or any other aspect of this collection of information, including suggestions for reducing this burden, to Department of Defense, Washington Headquarters Services, Directorate for Information Operations and Reports (0704-0188), 1215 Jefferson Davis Highway, Suite 1204, Arlington, VA 22202-4302. Respondents should be aware that notwithstanding any other provision of law, no person shall be subject to any penalty for failing to comply with a collection of information if it does not display a currently valid OMB control number.
PLEASE DO NOT RETURN YOUR FORM TO THE ABOVE ADDRESS.

1. REPORT DATE *(DD-MM-YYYY)* 01-09-2008	2. REPORT TYPE Technical Memorandum	3. DATES COVERED *(From - To)*

4. TITLE AND SUBTITLE
Turbulence Associated With Broadband Shock Noise in Hot Jets

5a. CONTRACT NUMBER

5b. GRANT NUMBER

5c. PROGRAM ELEMENT NUMBER

6. AUTHOR(S)
Bridges, James, E.; Wernet, Mark, P.

5d. PROJECT NUMBER

5e. TASK NUMBER

5f. WORK UNIT NUMBER
WBS 984754.02.07.03.17.02

7. PERFORMING ORGANIZATION NAME(S) AND ADDRESS(ES)
National Aeronautics and Space Administration
John H. Glenn Research Center at Lewis Field
Cleveland, Ohio 44135-3191

8. PERFORMING ORGANIZATION REPORT NUMBER
E-16544

9. SPONSORING/MONITORING AGENCY NAME(S) AND ADDRESS(ES)
National Aeronautics and Space Administration
Washington, DC 20546-0001

10. SPONSORING/MONITORS ACRONYM(S)
NASA

11. SPONSORING/MONITORING REPORT NUMBER
NASA/TM-2008-215274

12. DISTRIBUTION/AVAILABILITY STATEMENT
Unclassified-Unlimited
Subject Categories: 7 and 34
Available electronically at http://gltrs.grc.nasa.gov
This publication is available from the NASA Center for AeroSpace Information, 301-621-0390

13. SUPPLEMENTARY NOTES

14. ABSTRACT
Time-Resolved Particle Image Velocimetry (TRPIV) has been applied to a series of jet flows to measure turbulence statistics associated with broadband shock-associated noise (BBSN). Data were acquired in jets of Mach numbers 1.05, 1.185, and 1.4 at different temperatures. Both convergent and ideally expanded nozzles were tested, along with a convergent nozzle modified to minimize screech. Key findings include the effect of heat on shock structure and jet decay, the increase in turbulent velocity when screech is present, and the relative lack of spectral detail associated with the enhanced turbulence.

15. SUBJECT TERMS
Jet flow; Turbulence; Correlation; Jet aircraft noise; Particle image velocimetry; Velocity distribution; Prediction analysis techniques; Navier-Stokes equation; Laser anemometers; Velocity measurement; High resolution; Temperature effects

16. SECURITY CLASSIFICATION OF:			17. LIMITATION OF ABSTRACT	18. NUMBER OF PAGES	19a. NAME OF RESPONSIBLE PERSON STI Help Desk (email:help@sti.nasa.gov)
a. REPORT U	**b. ABSTRACT** U	**c. THIS PAGE** U	UU	27	19b. TELEPHONE NUMBER *(include area code)* 301-621-0390

Standard Form 298 (Rev. 8-98)
Prescribed by ANSI Std. Z39-18